

Analysing surface energy balance closure and partitioning over a semi-arid savanna FLUXNET site in Skukuza, Kruger National Park, South Africa

Nobuhle P. Majozi^{1,2}, Chris M. Mannaerts², Abel Ramoelo^{1,5}, Renaud Mathieu^{1,3}, Alecia Nickless⁴, Wouter Verhoef²

¹Earth Observation Group, Natural Resources and Environment, Council for Scientific and Industrial Research, Pretoria, South Africa, 0001

²Department of Water Resources, Faculty of Geo-Information Science and Earth Observation (ITC), University of Twente, Enschede, 75AA, the Netherlands

³Department of Geography, Geoinformatics and Meteorology, University of Pretoria, South Africa

⁴Nuffield Department of Primary Care Health Sciences, University of Oxford, Oxford, OX2 6GG, United Kingdom

⁵University of Limpopo, Risk and Vulnerability Centre, Sovenga, South Africa, 0727

Correspondence to: N. P. Majozi (nmajozi@csir.co.za)

Abstract

Flux towers provide essential terrestrial climate, water and radiation budget information needed for environmental monitoring and evaluation of climate change impacts on ecosystems and society in general. They are also intended for calibration and validation of satellite-based earth observation and monitoring efforts, such as assessment of evapotranspiration from land and vegetation surfaces using surface energy balance approaches.

In this paper, 15 years of Skukuza eddy covariance data, i.e. from 2000 to 2014, were analysed for surface energy balance closure (EBC) and partitioning. The surface energy balance closure was evaluated using the ordinary least squares regression (OLS) of turbulent energy fluxes (sensible (H) and latent heat (LE)) against available energy (net radiation (Rn) less soil heat (G)), and the energy balance ratio (EBR). Partitioning of the surface energy during the wet and dry seasons was [also](#) investigated, as well as how it is affected by atmospheric vapor pressure deficit (VPD), and net radiation.

After filtering years with [bad-low quality](#) data (2004-2008), our results show an overall mean EBR of 0.93. Seasonal variations of EBR also showed [summer-wet with 1.17](#) and spring (1.02) [being](#) closest to unity, with [winter-dry](#) (0.70) having the [highest imbalance](#). Nocturnal surface energy closure was very low at 0.26, and this was linked to low friction velocity during night-time, with results showing an increase in closure with increase in friction velocity.

The surface energy partitioning of this savanna ecosystem showed that sensible heat flux dominated the energy partitioning between March and October, followed by latent heat flux, and lastly the soil heat flux, and during the wet season where latent heat flux dominated sensible heat flux. An increase in net radiation was characterized by an increase in both LE and H, with LE showing a higher rate of increase than H in the wet season, and the reverse happening during the dry season. An increase in VPD is [correlated with](#) a decrease in LE and increase in H during the wet season, and an increase of both fluxes during the dry season.

1. Introduction

Net solar radiation (Rn) reaching the earth's surface determines the amount of energy available for latent (LE), sensible (H) and soil (G) heat fluxes, and heat stored by the canopy, the ground [and energy storage by photosynthesis](#). Energy partitioning on the earth's surface is a function of interactions between biogeochemical cycling, plant physiology, the state of the atmospheric boundary layer and climate (Wilson et al., 2002). How the turbulent fluxes (H and LE) are partitioned in an ecosystem plays a critical role in determining the hydrological cycle, boundary layer development, weather and climate (Falge et al., 2005). Understanding the partitioning of energy, particularly the turbulent fluxes, is important for water resource management in (semi) arid regions, where [potential-reference](#) evapotranspiration far exceeds precipitation.

49 Eddy covariance (EC) systems are currently the most reliable method for measuring carbon, energy and
50 water fluxes, and they have become a standard technique in the study of surface-atmosphere boundary layer
51 interactions. They provide a distinct contribution to the study of environmental, biological and climatological
52 controls of the net surface exchanges between the land surface (including vegetation) and the atmosphere
53 (Aubinet, et al., 1999; Baldocchi et al., 2001). The accuracy of these data is very important because they are used
54 to validate and assess performance of land surface and climate models. However, the EC techniques have
55 limitations in terms of data processing and quality control methods, especially under complex conditions (e.g.,
56 unfavorable weather, such as high turbulence and low wind speed, and heterogeneous topography). In EC
57 measurements, the ideal situation is that available energy, i.e. net radiation minus soil heat flux is equal to the sum
58 of the turbulent fluxes ($R_n - G = LE + H$); however, in most instances, the measured available energy is larger than
59 the sum of the ~~measurable-measured~~ turbulent fluxes of sensible heat and latent heat. Extensive research on the
60 issue of surface energy imbalance in EC observations has been done (Barr et al., 2012; Chen et al., 2009; Foken
61 et al., 2010; Franssen et al., 2010; Mauder et al., 2007), and closure error (or imbalance) has been documented to
62 be around 10-30 % ([Wilson et al., \(2002\)](#); [von Randow et al., \(2004\)](#); [Sanchez et al., \(2010\)](#)).

63 Causes for non-closure, [as extensively discussed](#), include unaccounted soil and canopy heat storage
64 [terms](#), non-inclusion of the low and high frequency turbulence in the computation of the turbulent fluxes, land
65 surface heterogeneities, systematic measurement and sampling errors. This imbalance has implications on how
66 energy flux measurements should be interpreted and how these estimates should be compared with model
67 simulations. The surface energy balance closure is an accepted performance criterion of EC flux data (Twine et
68 al., 2000; Wilson et al., 2002), and different methods have been used to assess the energy closure and partitioning,
69 including ordinary least squares regression (OLS) method, i.e. a plot of turbulence fluxes ($H + LE$) against available
70 energy ($R_n - G$), the residual method, i.e. $R_n - G - H - LE$, and the energy balance ratio, i.e. $(H + LE) / (R_n - G)$.

71 Several researchers have investigated surface energy partitioning and energy balance closure for different
72 ecosystems, including savannas. Bagayoko et al. (2007) examined the seasonal variation of the energy balance in
73 West African savannas, and noted that latent heat flux played a major role in the wet season, whereas sensible
74 heat flux was significant in the dry season. In the grassland Mongolian Plateau, Li et al. (2006) concluded that
75 sensible heat flux dominated the energy partitioning, followed by ground heat flux, with the rainy season showing
76 slight increase in latent heat flux. Gu et al. (2006) used different ratios (Bowen ratio, G/R_n , H/R_n and LE/R_n) to
77 investigate surface energy exchange in the Tibetan Plateau, and showed that during the vegetation growth period,
78 LE was higher than H , and this was reversed during the post-growth period.

79 Research using the Skukuza EC system data has focused mainly on the carbon exchange, fire regimes, and
80 in global analysis of the energy balance (Archibald et al., 2009; Kutsch et al., 2008; Williams et al., 2009).
81 However, there has been no investigation of surface energy partitioning and energy balance closure in this
82 ecosystem. In this study, we examined the surface energy balance partitioning into soil heat conduction,
83 convection (sensible) and latent heat components and its energy balance closure using 15 years (2000-2014) of
84 eddy covariance data from the Skukuza flux tower.

85 First, a multi-year surface energy balance closure (EBC) analysis was done, including the seasonal and day-
86 night EBC evaluations, and an assessment of its error sources. This included investigating how friction velocity
87 affects the closure, and its link to low nighttime EBC. [Then we examined how the surface energy partitioning](#)
88 [varies over time in this ecosystem, based on the climate conditions in the region, particularly, in relation to water](#)

89 [availability \(precipitation\) and vegetation dynamics. The effect of VPD and Rn on surface energy partitioning](#)
90 [between turbulent fluxes](#), during the wet and dry seasons was [also](#) examined. [Through this study, we expect to](#)
91 [contribute to existing literature on the surface energy balance closure and partitioning, especially in savanna sites.](#)
92

93 **2. Materials and methods**

94 **2.1. Site description**

95 The Skukuza flux tower (25.02°S, 31.50°E) was established early 2000 as part of the SAFARI 2000 campaign
96 and experiment, set up to understand the interactions between the atmosphere and the land surface in Southern
97 Africa by connecting ground data of carbon, water, and energy fluxes with remote sensing data generated by Earth
98 observing satellites (Scholes et al., 2001; Shugart et al., 2004).

99 The site is located in the Kruger National Park (South Africa) at 365 m above sea level, and receives 550
100 ± 160 mm precipitation per annum between November and April, with significant inter-annual variability. The
101 year is divided into a hot, wet growing season and a warm, dry non-growing season. The soils are generally
102 shallow, with coarse sandy to sandy loam textures (about 65 % sand, 30 % clay and 5% silt). The area is
103 characterized by a catenal pattern of soils and vegetation, with broad-leaved *Combretum* savanna on the crests
104 dominated by the small trees (*Combretum apiculatum*), and fine-leaved *Acacia* savanna in the valleys dominated
105 by *Acacia nigrescens* (Scholes et al., 1999). The vegetation is mainly open woodland, with approximately 30 %
106 tree canopy cover of mixed *Acacia* and *Combretum* savanna types. Tree canopy height is 5–8 m with occasional
107 trees (mostly *Sclerocarya birrea*) reaching 10 m. The grassy and herbaceous understory comprises grasses such
108 as *Panicum maximum*, *Digitaria eriantha*, *Eragrostis rigidor*, and *Pogonarthria squarrosa*.

109 **2.1.1. Eddy covariance system**

110 Since 2000, ecosystem-level fluxes of water, heat and carbon dioxide are measured using an eddy covariance
111 system mounted at 16 m height of the 22 m high flux tower. The measurements taken and the instruments used
112 are summarized in Table 1.

113 **(Table 1)**

114 From 2000 to 2005, H and LE were derived from a closed-path CO₂/H₂O monitoring system, which was replaced
115 by the open-path gas analyzer in 2006. Also, from 2000 to 2008, incident and reflected shortwave radiation (i.e.
116 300–1100 nm, Wm⁻²), incident and reflected near-infrared (600–1100 nm, Wm⁻²) and incoming and emitted
117 longwave radiation (>3.0 μm, Wm⁻²) measurements were made using a two-component net radiometer (Model
118 CNR 2: Kipp & Zonen, Delft, The Netherlands) at 20 s intervals and then recorded in the data-logger as 30 min
119 averages; this was replaced with the Kipp & Zonen NRLite net radiometer in 2009. Soil heat flux is measured
120 using the HFT3 plates (Campbell Scientific) installed at 5 cm below the surface at three locations, two under tree
121 canopies and one between canopies.

122 Ancillary meteorological measurements include air temperature and relative humidity, also measured at
123 16 m height, using a Campbell Scientific HMP50 probe; precipitation at the top of the tower using a Texas
124 TR525M tipping bucket rain gauge; wind speed and direction using a Climatronics Wind Sensor; and soil
125 temperature using Campbell Scientific 107 soil temperature probe.
126
127

2.1.2. Data pre-processing

The Eddysoft software was used to process the raw data collected from the eddy covariance system (Kolle & Rebmann, 2007). Post-processing of the raw high frequency (10 Hz) data for calculation of half-hour periods of the turbulent fluxes and CO₂ (F_c; g CO₂ m⁻² time⁻¹) involved standard spike filtering, planar rotation of velocities and lag correction to CO₂ and q (Aubinet et al., 1999; Wilczak et al., 2001). Frequency response correction of some of the energy lost due to instrument separation, tube attenuation, and gas analyzer response for LE and F_c was performed with empirical co-spectral adjustment to match the H co-spectrum (Eugster and Senn, 1995; Su et al., 2004).

2.2. Data analysis

Half-hourly measurements of eddy covariance and climatological data from 2000 to 2014 were used to assess surface energy partitioning and closure. When measuring the different variables, instruments like the sonic anemometer and the net radiometer are affected by different phenomena, like rainfall events and wind gusts, resulting in faulty diagnostic signals, outliers and data gaps, which are sources of error and bias. Thus cleaning, which involved screening, diagnosing and editing, of these half-hourly surface energy data, which was done to reduce bias and error, rejected i) data from periods of sensor malfunction (i.e. when there was a faulty diagnostic signal), (ii) incomplete 30-minute datasets of R_n, G, LE and H, and iii) outliers. The data outliers were detected using the outlier detection procedure found in the Statistica software. After data screening, flux data with non-missing values of R_n, G, LE and H data were arranged according to monthly and seasonal periods (summer (December – February), autumn (March – May), winter (June – August), and spring (September – November)), as well as into daytime and nighttime.

Soil heat flux was then computed as a weighted mean of the three measurements, i.e., two taken under tree canopies and one on open space.

2.2.1. Surface energy balance assessment

The law of conservation of energy states that energy can neither be created nor destroyed, but is transformed from one form to another, hence the ideal surface energy balance equation is written as:

$$R_n - G = H + LE \quad (1)$$

Energy imbalance occurs when both sides of the equation do not balance. The energy balance closure was evaluated at different levels, i.e. multi-year, seasonal, and day/ night periods (the assumption being that daytime has positive R_n and nighttime has negative R_n), using two methods, i.e.

i) The ordinary least squares method (OLS), which is the regression between turbulent fluxes and available energy.

Ideal closure is when the intercept is zero and slope and the coefficient of determination (R²) are one. An assumption is made using this method, that there are no random errors in the independent variables, i.e. R_n and G, which of course is an incorrect assumption a simplification.

ii) The energy balance ratio (EBR), which is ratio of the sum of turbulent fluxes to the available energy, $\Sigma(LE + H)/\Sigma(R_n - G)$.

The EBR gives an overall evaluation of energy balance closure at longer time scales by averaging over errors in the half-hour measurements; and the ideal closure is 1. EBR has the potential to remove biases in the half-hourly

168 data, such as the tendency to overestimate positive fluxes during the day and underestimate negative fluxes at
169 night. [We did not account for the heat storage terms in the EBR, including soil and canopy heat storage, and](#)
170 [energy storage by photosynthesis and respiration, in this study. The significance of neglecting these storage terms](#)
171 [will be discussed.](#)

172 To investigate the effect of friction velocity on EBR and how it is related to time of day, using friction
173 velocity, the [half-hourly](#) data were separated into [four](#) 25-percentiles, and the EBR and OLS evaluated. [Matlab](#)
174 [was used to create the graphs.](#)

176 2.2.2. Analyzing surface energy partitioning

177 To evaluate solar radiation variation and partitioning into latent and sensible heat fluxes in this biome, EC surface
178 energy data from 2000 to 2014 were used. [Violations in micrometeorological assumptions, instrument](#)
179 [malfunction and poor weather result in a proportion of the data being rejected. Yet, our aim was to construct](#)
180 [continuous records of half-hourly fluxes measured by eddy covariance and compute monthly, seasonal and annual](#)
181 [sums of surface energy fluxes. To fill the gaps in our dataset, we used the Amelia II software, an R-program](#)
182 [designed to impute missing data using Expectation-Maximization with Bootstrapping \(EMB\) multiple imputation](#)
183 [algorithm \(Honaker et al., 2011\). The original dataset is resampled using bootstrapping, after which the missing](#)
184 [data values are imputed using Expectation-Maximization algorithm. Each complete imputed dataset is in such a](#)
185 [way that the observed values are the same as those in the original data set; only the missing values are different.](#)

186 The minimum, maximum and mean statistics of Rn, H, LE and G were then estimated. The monthly and
187 seasonal trends of energy partitioning were assessed, [and how each component is affected by vegetation dynamics](#)
188 [at the site.](#) Surface energy partitioning was also characterized as a direct function of vapor pressure deficit (VPD)
189 and Rn during the wet and dry seasons, [following Gu et al. \(2006\).](#)

191 3. Results and Discussion

192 3.1. Meteorological conditions

193 Fig 1 shows the 15-year [average-daily-mean monthly anomalies of air](#) temperature, VPD and rainfall totals at the
194 Skukuza flux tower [site](#). The annual average temperatures over the 15-year period ranged between 21.13°C in
195 2012 and 23.23 °C in 2003, with a 15-year average temperature of 22.9 °C. While 2003 was the hottest year, it
196 was also the driest year, with annual rainfall of 273.6 mm, with 2002 also recording very low rainfall of 325.4
197 mm, both receiving rainfall amounts below the recorded mean annual rainfall of 550±160 mm. The wettest years
198 were 2013, 2000, 2014 and 2004 which received 1414, 1115.6, 1010.2 and 1005.7 mm, respectively. 2007 and
199 2008 had incomplete rainfall data records to assess their annuals. The annual daily average VPD was between
200 0.024 and 4.03 kPa, with an overall average of 1.28 ± 0.62 kPa. The daily average VPD decreased with rainy
201 days, and showed an increase during rain-free days. The wet years, i.e. 2000, 2013 and 2014 had low annual
202 average VPD of 1.98, 1.34 and 1.83 kPa, respectively, whereas the drought years exhibited high VPDs with 2002
203 and 2003 with 2.77 and 2.97 kPa, respectively. The long-term weather records are comparable with the 1912 –
204 2001 and 1960 – 1999 climate analysis for the same area as reported by Kruger et al. (2002) and Scholes et al.
205 (2001), showing a mean annual total precipitation of 547.1 mm and air temperature of 21.9 °C. The low rainfall
206 during 2000-2003 seasons was also reported by Kutch et al. (2008), who were investigating the connection
207 between water relations and carbon fluxes during the mentioned period.

208 **(Figure 1)**

209

210 3.2. Surface energy balance assessment

211 Data completeness varied largely [7.59 % \(2006\)](#) and [67.97 % \(2013\)](#), with a mean of [34.84 %](#). The variation in
212 data completeness is due to a number of factors including instrument failures, changes and (re)calibration, and
213 poor weather conditions.

214

215 3.2.1. Multi-year analysis of surface energy balance closure

216 Fig 2 summarizes results of the multi-year energy balance closure analysis for the Skukuza eddy covariance
217 system from 2000 to 2014. The coefficient of determination (R^2) for the 15-years period varied between 0.74 and
218 0.92, with a mean value of 0.85 ± 0.06 . The slopes ranged between 0.56 and 1.25, with a mean 0.77 ± 0.19 , while
219 the intercepts varied from -23.73 to 26.28, with a mean of 1.03 ~~with-and~~ standard deviation of 18.20 Wm^{-2} . The
220 annual energy balance ratio (EBR) for the 15 years ~~extended~~ between 0.44 in [2005 and 2007](#) and [1.09 in 2011](#),
221 with a mean of 0.78 ± 0.24 . Between 2004 and 2008, EBR ~~ranged~~s between 0.44 and 0.53, whereas from 2000 to
222 2003 and 2009 to 2014, the EBR ~~ranged-was between~~ 0.76 and 1.09. The EBR for 2010 to 2012 were slightly
223 greater than 1 ([1.08, 1.09 and 1.01, respectively](#)), indicating an overestimation of the turbulent fluxes (H+LE)
224 compared to the available energy, [this still giving the absolute imbalance values of within 30 %](#). The remaining
225 years, [2000-2003 and 2009](#), were less than 1, indicating that the turbulent fluxes were lower than the available
226 energy. [The further away the slope is from unity, the lower the EBR, as shown by the low slope values between](#)
227 [2004 and 2008](#). The period of low EBR between 2004 and 2008 is characterized by the absence of negative values
228 of available energy ($R_n - G$) as illustrated in Fig 2. Between 2000 and 2004, the CNR2 net radiometer was used to
229 measure long and shortwave radiation, and these were combined to derive R_n . However, when the pyrgeometer
230 broke down in 2004, R_n was derived from measured shortwave radiation and modelled longwave radiation until
231 the CNR2 was replaced by the NRLite net radiometer in 2009. This was a significant source of error, as shown
232 by the low EBR between 2004 and 2008. The closed-path gas analyzer was also changed to open-path gas analyzer
233 in 2006. An analysis of the 2006 data (which had very low data completeness of 7.59 %) showed that there were
234 no measurements recorded until September, possibly due to instrument failure. [Further analysis and discussion of](#)
235 [the EBR was done with the exclusion of years with low quality data.](#)

236 Our final mean multiyear EBR estimate, excluding the years with [poor data quality](#) (2004 to 2008), was
237 therefore 0.93 ± 0.11 , [ranging between 0.76 and 1.09](#). [The \$R^2\$ for these years varied between 0.77 and 0.92, with](#)
238 [a mean value of \$0.87 \pm 0.05\$. The slopes were from 0.7 to 1.25, with a mean \$0.87 \pm 0.17\$, while the intercepts varied](#)
239 [from -12.57 to 26.28, with a mean of 10.79 and standard deviation of \$13.67 \text{ Wm}^{-2}\$.](#)

240 **(Figure 2)**

241 The EBR results for the Skukuza eddy covariance system, [which vary between 0.76 and 1.09](#) with an [annual](#) mean
242 of 0.93 (only the years with [high quality](#) data), are generally within the reported accuracies [as shown in](#) most
243 studies that report the energy balance closure error at 10–30% [, across different ecosystems](#). [For instance](#), Wilson
244 et al., (2002) also [recorded an annual](#) mean EBR of 0.84, ranging [between 0.34 and 1.69 in an extensive study](#)
245 [investigating 22 FLUXNET sites across the globe; EBR in ChinaFLUX sites ranged between 0.58 and 1.00, with](#)
246 [a mean of 0.83 \(Yuling et al., 2005\); according to](#) Were et al. (2007), ~~reported~~ EBR values of about 0.90 [were](#)
247 [found](#) over shrub and herbaceous patches, in a dry valley in southeast Spain, ~~whereas~~ Chen et al. (2009) ~~report~~
248 [showed](#) a mean of 0.98 EBR for their study in the semi-arid region of Mongolia, [and](#) an EBR value of 0.80 was

249 found by Xin and Liu (2010) in a maize crop [in semi-arid conditions, in China](#). Using data from the Tibetan
250 Observation and Research Platform (TORP), Liu et al. (2011) observed an EBR value of 0.85 in an alfalfa field
251 in semi-arid China.

253 3.2.2. Seasonal variation of EBR

254 Fig 3 shows the seasonal OLS results for the 15 year period, excluding years 2004 to 2008. The slopes ranged
255 between 0.94-67 and 1.21-0.87, with a mean of 1.10 ± 0.11 and 0.78 ± 0.08 , and the intercepts were a mean of 11.97 and 19.13
256 $\text{Wm}^{-2} \pm 3.87$ and 16.30Wm^{-2} . R^2 ranged between 0.81 and 0.88 with a mean of 0.84 ± 0.04 . The EBR for the different
257 seasons ranged between 0.70 and 1.12, with a mean of 0.92 ± 0.19 . The ~~winter-dry~~ season had the lowest EBR of
258 0.70, while summer recorded 1.02, and spring were closest to unity with EBR of ~~-~~ and 1.12, respectively, and
259 autumn had EBR of 0.84. A large number of outliers is observed in summer due to cloudy weather conditions and
260 rainfall events that make the thermopile surface wet, thus reducing the accuracy of the net radiometer. A study
261 comparing different the performance of different net radiometers by Blonquist et al. (2009) shows that the NR-
262 Lite is highly sensitive to precipitation and dew/ frost since ~~+~~the sensor is not protected.

263 (Figure 3)

264 [The results of our study concur with similar studies that assessed the seasonal variation of EBR. For instance,](#)
265 Wilson et al. (2002) comprehensively investigated the energy closure of the summer and winter seasons for 22
266 FLUXNET sites for 50 site-years. They also reported higher energy balance correlation during the wet compared
267 to the dry season, with the mean R^2 of 0.89 and 0.68, respectively. [Whereas our results show significant differences](#)
268 [between the wet \(1.12\) and dry \(0.70\)-their, their](#) EBR showed smaller differences between the two seasons, being
269 0.81 and 0.72, for summer and winter, respectively. Ma et al. (2009) reported an opposite result from the Skukuza
270 results, showing energy closures of 0.70 in summer and 0.92 in winter over the flat prairie on the northern Tibetan
271 Plateau.

273 3.2.3. Day – night-time effects

274 Fig 4 shows the daytime and nocturnal OLS regression results for the 15 year period. The daytime and nocturnal
275 slopes were 0.99 and 0.11, with the intercepts being 76.76 and 1.74 Wm^{-2} , respectively. Daytime and nocturnal
276 R^2 were 0.64 and 0.01, respectively. The EBR for the different times of day were 0.96 and 0.27, daytime and
277 nocturnal, respectively.

278 (Figure 4)

279 Other studies also reported a higher daytime surface energy balance closure. For instance, Wilson et al., (2002)
280 showed that the mean annual daytime EBR was 0.8, whereas the nocturnal EBR was reported to be was negative
281 or was much less or much greater than 1.

282 To understand the effect of friction velocity on the energy balance closure, [surface energy data](#) which
283 had [corresponding](#) friction velocity (u^*) data, were used. Using friction velocity, the data were separated into 4
284 25-percentiles, and the EBR and OLS evaluated. Results show that the first quartile, the EBR was 3.94, with the
285 50-percentile at 0.99, the third quartile at unity, and the fourth quartile at 1.03 (Fig 5). The slopes were between
286 1.01 and 1.12, with the intercepts ranging between -9.26 and -0.17 Wm^{-2} , whereas R^2 were 0.82, 0.86, 0.85 and
287 0.81 for the first to the fourth quartiles, respectively.

288 (Figure 5)

289 An assessment shows that the time associated with the low friction velocities, i.e. the first quartile are night-time
290 data constituting 81 % of the whole first quartile dataset, and the last quartile had the highest number of daytime
291 values at 79.29 % of the fourth quartile dataset. Lee and Hu (2002) hypothesized that the lack of energy balance
292 closure during nocturnal periods was often the result of mean vertical advection, whereas Aubinet et al.,
293 (1999) and Blanken et al., (1997) showed that energy imbalance during nocturnal periods is usually greatest when
294 friction velocity is small. Another source of error in the nocturnal EBR is the high uncertainty in night-time
295 measurements of R_n . At night, the assumption is that there is no shortwave radiation, and R_n is a product of
296 longwave radiation. Studies show that night-time measurements of longwave radiation were less accurate than
297 daytime measurements (Blonquist et al., 2009). The RN-Lite, for instance has low sensitivity to longwave
298 radiation, resulting in low accuracy in low measurements.

299 Soil heat flux (G) plays a significant role in the surface energy balance as it determined how much energy
300 is available for the turbulent fluxes, especially in areas with limited vegetation cover. In this study, we examined
301 how G , i.e., its presence or absence, impacts on the EBR. Our results revealed a decrease of up to 7 %, with an
302 annual mean of 3.13 ± 2.70 , in EBR when G was not included in the calculation. During the daytime, the absence
303 of G resulted in a decrease of approximately 10 % of the initial EBR, while at nighttime EBR was as low as 50 %
304 of the initial EBR, showing that G has greater impact on the surface energy balance at night. While G plays a
305 significant role on the surface energy balance closure, our study ignored the different energy storage terms in
306 determining the EBR, including the soil heat storage. The exclusion of the soil heat storage results in the
307 underestimation of G , as the real value of G is a combination of the flux measured by the plate and the heat
308 exchange between the ground and the depth of the plate. This in turn contributes to overestimating the available
309 energy, which then lowers the EBC. As reported by different studies, the omission of the soil heat storage results
310 in the underestimation of the energy EBC by up to 7 %. For instance, Zuo et al. (2011) reported an improvement
311 of 6 to 7 % when they included the soil heat storage in their calculation of EBR., at the Semi-Arid Climate and
312 Environment Observatory of Lan-Zhou University (SACOL) site in semi-arid grassland over the Loess Plateau
313 of China. In their study in the three sites in the Badan Jaran desert, Li, Liu, Wang, Miao, and Chen (2014) analysed
314 the effect of including soil heat storage derived by different methods in the energy balance closure; their EBR
315 improved by between 1.5 % and 4 %. The improvement of the EBR in the study in a FLUXNET boreal site in
316 Finland by Sánchez, Caselles, and Rubio (2010) was shown to be 3 % when the soil heat storage was included,
317 which increased to 6 % when other storage terms (canopy air) were taken into account.

319 3.3. Surface energy partitioning

320 3.3.1. Surface energy measurements

321 The mean daily and annual measurements of the energy budget components from 2000 to 2014 are highlighted in
322 Fig 6 and Table 2. The seasonal cycle of each component can be seen throughout the years, where at the beginning
323 of each year the energy budget components are high, and as each year progresses they all decrease to reach a low
324 during the middle of the year, which is the winter/ dry season, and a gradual increase being experienced during
325 spring right to the summer at the end of each year. The multi-year daily means of R_n , H , LE and G were 139.1
326 Wm^{-2} , $57.70 Wm^{-2}$, $42.81 Wm^{-2}$ and $2.94 Wm^{-2}$, with standard deviations of $239.75 Wm^{-2}$, $104.15 Wm^{-2}$, 70.58
327 Wm^{-2} and $53.67 Wm^{-2}$, respectively.

328 (Figure 6)

329 The gaps in 2006 indicate the absence of the surface energy flux measurements in those years, which was a result
330 of instrument failure. Between 2004 and 2008, the Rn was calculated as a product of measured shortwave radiation
331 and modelled longwave radiation, which was a high source of error in the estimation of Rn. These years are also
332 ~~characterised~~characterized by poor energy balance closure, as shown in Section 3.2.1 above.

333 (Table 2)

334

335 3.3.2. Influence of weather conditions and seasonality

336 In arid/semi-arid ecosystems, solar radiation is not a limiting factor for [latent heat flux](#), instead it is mainly limited
337 by water availability. The seasonal fluctuations of energy fluxes are affected by the seasonal changes in the solar
338 radiation, air temperature, precipitation and soil moisture (Baldocchi et al., 2000; Arain et al., 2003). These
339 climatic variables influence vegetation dynamics in an ecosystem, as well as how solar radiation is partitioned.
340 Hence, daily measurements of precipitation, air temperature and VPD were evaluated to investigate the
341 partitioning of the surface energy in the semi-arid savanna landscape of Skukuza.

342 (Figure 7)

343 To illustrate the partitioning of solar radiation into the different fluxes throughout the year, Fig 7 presents
344 the multi-year mean monthly variations of the surface energy components showing a general decrease of the
345 components between February and June, which then gradually increases again until November. The multi-year
346 monthly means of Rn, H, LE and G were 71.27 Wm⁻² (June) and 197.33 Wm⁻² (November), 37.11 Wm⁻² (June)
347 and 80.37 Wm⁻² (November), 8.52 Wm⁻² (August) and 127.17 Wm⁻² (December), -2.28 Wm⁻² (June) and 20.78
348 Wm⁻² (November), respectively. The month of August had the highest BR of 6.42, whereas December had the
349 least at 0.42. The residual accounted for between ~~-19.69 and~~ 34.74 % of Rn, and an average of 4.70 %.

350 The general trend shows that sensible heat flux dominated the energy partitioning between May and
351 October, followed by latent heat flux, and lastly the soil heat flux, except during the wet season where latent heat
352 flux was larger than sensible heat flux. This is illustrated by the trend of BR, [showing an](#) increase from April, with
353 the peak in August, then a steady decrease until it hits lowest in December. The period of low BR is
354 ~~characterised~~characterized by high Rn and high precipitation. As the season transitions into ~~winter~~the dry season,
355 it is ~~characterised~~characterized by reduced net radiation and low measurements H and LE.

356 Just before the first rains, i.e. between September and November, tree flowering and leaf emergence
357 occurs in the semi-arid savanna in the Skukuza area (Archibald and Scholes, 2007), and grasses shoot as soil
358 moisture availability improves with the rains (Scholes et al., 2003). This is ~~characterised~~characterized by a gradual
359 increase in LE and decrease in BR, which, when compared to the ~~winter-dry~~ dry season, is significantly lower than
360 the H, as illustrated in Fig 7. As the rainy season progresses, and vegetation development peaks, [LE](#) also reaches
361 its maximum, becoming significantly higher than [H](#), and hence, [low](#) BR. Between March and September, when
362 leaf senescence occurs, the leaves gradually change colour to brown and grass to straw, and trees defoliate, [H](#)
363 again gradually becomes significantly higher than LE.

364 (Figure 8)

365 The influence of VPD and Rn on surface energy partitioning was investigated during the wet and dry
366 seasons. Results show [that during both periods](#) there is an increase in H and decrease in LE with an increase in
367 VPD; [although the gradient of LE rise differ significantly during the two periods, H increases similarly during](#)
368 [both the wet and dry periods](#) (Fig 89). VPD is higher [in times of](#) little or no rain (low soil water availability),

369 which explains the [slight increase in LE](#) with a rise [in](#) VPD (Fig [9d](#)). In this instance, although the evaporative
370 demand is high, the stomatal conductance is reduced due to absence of water in the soil, resulting in smaller LE
371 and higher H. Rn, on the other hand, is partitioned into different fluxes, based on other climatic and vegetation
372 physiological characteristics. [Figure 9](#) illustrates that both LE and H increase with increase in Rn, although their
373 increases are not in proportion, based on season. During the wet season, the rate of increase of LE is higher than
374 that of H, whereas in the dry season the reverse is true. The rate of increase of LE is controlled by the availability
375 of soil water (precipitation), (also illustrated in [Figure 6](#) (LE)), and during the wet season it increases steadily with
376 increasing Rn, whereas the rate of increase of H is concave, showing saturation with an increase in Rn. The
377 opposite is true during the dry season, with limited water availability, [where](#) the rate of increase of LE slows down
378 with increase in Rn, and a steady increase of H with Rn increase.

379 [\(Figure 9\)](#)

380 [Our study results are consistent with similar studies, for example](#) [Gu, Gu et al. \(2006\)](#), [who](#) examined
381 how soil moisture, vapor pressure deficit (VPD) and net radiation control surface energy partitioning at a
382 temperate deciduous forest site in central Missouri, USA. [Both studies agree that](#) with ample soil moisture, [during](#)
383 [the rainy season](#), latent heat flux dominates over sensible heat flux, and reduced soil [water](#) availability reversed
384 the dominance of latent heat over sensible heat, because of its direct effect on stomatal conductance. An increase
385 in net radiation, on the other hand, also increases both sensible and latent heat fluxes. The increase of either then
386 becomes a function of soil moisture availability, since they cannot increase in the same proportion. However,
387 [whereas we found that a rise in VPD is characterized by a decrease in LE and an increase in H in both periods](#),
388 their findings [show a](#) significant increase in LE and decrease in H with a rise in VPD during the non-drought
389 period, [with both components showing slight increases with increase in VPD](#) in dry conditions. Li et al. (2012)
390 also investigated the partitioning of surface energy in the grazing lands of Mongolia, and concluded that the energy
391 partitioning was also controlled by vegetation dynamics and soil moisture availability, although soil heat flux is
392 reportedly higher than latent heat flux in most instances. In a temperate mountain grassland in Austria, [Harmmerle](#)
393 [et al., \(2008\)](#) found that the energy partitioning in this climatic region was dominated by latent heat flux, followed
394 by sensible heat flux and lastly soil heat flux.

395 The consensus in all above studies is that vegetation and climate dynamics play a critical role in energy
396 partitioning. They note that during full vegetation cover, latent heat flux is the dominant portion of net radiation.
397 However, depending on the climatic region, the limiting factors of energy partitioning vary between water
398 availability and radiation. Our study confirms that in semi-arid regions, sensible heat flux is the highest fraction
399 of net radiation throughout the year, except during the wet period, when latent heat flux surpasses sensible heat
400 flux. However, in regions and locations where water availability is not a limiting factor, latent heat flux may take
401 the highest portion of net radiation.

402 403 **4. Conclusion**

404 This study investigated both surface energy balance and ~~its~~ [how it is partitioning-partitioned](#) into turbulent fluxes
405 during the wet and dry seasons in a semi-arid savanna ecosystem in Skukuza using eddy covariance data from
406 2000 to 2014. The analysis revealed a mean multi-year energy balance ratio of 0.93, ~~The~~ [the](#) variation of RBR
407 based on season, time of day and as a function of friction velocity was explored. The seasonal EBR varied between
408 0.70 and [1.12](#), with ~~winter~~ [the dry season](#) recording the highest energy imbalance. Daytime EBR was as high as

409 0.96, with 0.27 EBR for the nighttime. The high energy imbalance at night was explained as a result of stable
410 conditions, which limit turbulence that is essential for the creation of eddies. The assessment of the effect of
411 friction velocity on EBR showed that EBR increased with an increase in friction velocity, with low friction
412 velocity experienced mainly during night-time.

413 The energy partition analysis revealed that sensible heat flux is the dominant portion of net radiation in
414 this semi-arid region, except ~~in summer, when there is rainfall~~during the rainfall period. The results also show
415 that water availability and vegetation dynamics play a critical role in energy partitioning, whereby when it rains,
416 vegetation growth occurs, leading to an increase in latent heat flux / evapotranspiration. Clearly an increase in Rn
417 results in a rise in H and LE, however their increases are controlled by water availability. During the wet season,
418 the rate of increase of LE is higher than that of H, whereas in the dry season the reverse is true. The rate of increase
419 of LE is controlled by the availability of soil water (precipitation), and during the wet season it increases steadily
420 with increasing Rn, whereas the rate of increase of H shows saturation with an increase in Rn. The opposite is
421 true during the dry season, with limited water availability, the rate of increase of LE reaches saturation with
422 increase in Rn and a steady increase of H with Rn increase. An increase in VPD, on the other hand, results in an
423 increase in H and decrease in LE, with higher VPD experienced during the dry season, which explains the high
424 H, although the evaporative demand is high.

425

426 **Acknowledgements**

427 This study was supported by the Council for Scientific and Industrial Research under the project entitled
428 “Monitoring of water availability using geo-spatial data and earth observations”, and the National Research
429 Foundation under the Thuthuka PhD cycle grant.

430

431 **References**

432 Archibald, S., & Scholes, R. (2007). Leaf green-up in a semi-arid ~~afriean~~African savanna-separating tree and grass
433 responses to environmental cues. *Journal of Vegetation Science*, 18(4), 583-594.

434 Archibald, S., Kirton, A., Merwe, M., Scholes, R., Williams, C., & Hanan, N. (2009). Drivers of inter-annual
435 variability in net ecosystem exchange in a semi-arid savanna ecosystem, South ~~afriean~~Africa. *Biogeosciences*, 6(2),
436 251-266.

437 Aubinet, M., Grelle, A., Ibrom, A., Rannik, Ü., Moncrieff, J., Foken, T., . . . Bernhofer, C. (1999). Estimates of
438 the annual net carbon and water exchange of forests: The EUROFLUX methodology. *Advances in Ecological
439 Research*, 30, 113-175.

440 Bagayoko, F., Yonkeu, S., Elbers, J., & van de Giesen, N. (2007). Energy partitioning over the West African
441 savanna: Multi-year evaporation and surface conductance measurements in eastern ~~burkina~~Burkina fasoFaso.
442 *Journal of Hydrology*, 334(3), 545-559.

443 Baldocchi, D., Falge, E., Gu, L., Olson, R., Hollinger, D., Running, S., . . . Evans, R. (2001). FLUXNET: A new
444 tool to study the temporal and spatial variability of ecosystem-scale carbon dioxide, water vapor, and energy flux
445 densities. *Bulletin of the American Meteorological Society*, 82(11), 2415-2434.

446 Barr, A. G., van der Kamp, G., Black, T. A., McCaughey, J. H., & Nestic, Z. (2012). Energy balance closure at
447 the BERMS flux towers in relation to the water balance of the White Gull Creek watershed 1999–2009.
448 *Agricultural and Forest Meteorology*, 153(0), 3-13.

449 Blanken, P., Black, T. A., Yang, P., Neumann, H., Nesic, Z., Staebler, R., . . . Lee, X. (1997). Energy balance and
450 canopy conductance of a boreal aspen forest: Partitioning overstory and understory components. *Journal of*
451 *Geophysical Research: Atmospheres* (1984–2012), 102(D24), 28915-28927.

452 Blonquist, J., et al. (2009). "Evaluation of measurement accuracy and comparison of two new and three traditional
453 net radiometers." *Agricultural and Forest Meteorology* **149**(10): 1709-1721.

454 Chen, S., Chen, J., Lin, G., Zhang, W., Miao, H., Wei, L., . . . Han, X. (2009). Energy balance and partition in
455 inner Mongolia steppe ecosystems with different land use types. *Agricultural and Forest Meteorology*, 149(11),
456 1800-1809.

457 Eugster, W., & Senn, W. (1995). A cospectral correction model for measurement of turbulent NO₂ flux. *Boundary-*
458 *Layer Meteorology*, 74(4), 321-340.

459 Falge, E., Reth, S., Brüggemann, N., Butterbach-Bahl, K., Goldberg, V., Oltchev, A., . . . Queck, R. (2005).
460 Comparison of surface energy exchange models with eddy flux data in forest and grassland ecosystems of
461 [germanyGermany](#). *Ecological Modelling*, 188(2), 174-216.

462 Foken, T., Mauder, M., Liebethal, C., Wimmer, F., Beyrich, F., Leps, J., . . . Bange, J. (2010). Energy balance
463 closure for the LITFASS-2003 experiment. *Theoretical and Applied Climatology*, 101(1-2), 149-160.

464 Franssen, H., Stöckli, R., Lehner, I., Rotenberg, E., & Seneviratne, S. (2010). Energy balance closure of eddy-
465 covariance data: A multisite analysis for [europeanEuropean](#) FLUXNET stations. *Agricultural and Forest*
466 *Meteorology*, 150(12), 1553-1567.

467 Goosse H., P.Y. Barriat, W. Lefebvre, M.F. Loutre and V. Zunuz, (2008-2010). Introduction to climate dynamics
468 and climate modeling. Online textbook available at <http://www.climate.be/textbook>.

469 Gu, L., Meyers, T., Pallardy, S. G., Hanson, P. J., Yang, B., Heuer, M., . . . Wullschlegel, S. D. (2006). Direct
470 and indirect effects of atmospheric conditions and soil moisture on surface energy partitioning revealed by a
471 prolonged drought at a temperate forest site. *Journal of Geophysical Research: Atmospheres* (1984–2012),
472 111(D16)

473 Hammerle, A., Haslwanter, A., Tappeiner, U., Cernusca, A., & Wohlfahrt, G. (2008). Leaf area controls on energy
474 partitioning of a temperate mountain grassland. *Biogeosciences (Online)*, 5(2).

475 Honaker, J., et al. (2011). "Amelia II: A program for missing data." *Journal of statistical software* 45(7): 1-47.

476 Kolle, O., & Rebmann, C. (2007). EddySoft: Dokumentation of a Software Package to Acquire and Process Eddy
477 Covariance Data.

478 Kutsch, W., Hanan, N., Scholes, R., McHugh, I., Kubheka, W., Eckhardt, H., & Williams, C. (2008). Response
479 of carbon fluxes to water relations in a savanna ecosystem in [sSouth africaAfrica](#). *Biogeosciences Discussions*,
480 5(3), 2197-2235.

481 Li, S., Eugster, W., Asanuma, J., Kotani, A., Davaa, G., Oyunbaatar, D., & Sugita, M. (2006). Energy partitioning
482 and its biophysical controls above a grazing steppe in central [mongoliaMongolia](#). *Agricultural and Forest*
483 *Meteorology*, 137(1), 89-106.

484 [Li, Y., Liu, S., Wang, S., Miao, Y., & Chen, B. \(2014\). Comparative study on methods for computing soil heat](#)
485 [storage and energy balance in arid and semi-arid areas. *Journal of Meteorological Research*, 28, 308-](#)
486 [322.](#)

487 Liu, S., Xu, Z., Wang, W., Jia, Z., Zhu, M., Bai, J., & Wang, J. (2011). A comparison of eddy-covariance and
488 large aperture scintillometer measurements with respect to the energy balance closure problem. *Hydrology and*
489 *Earth System Sciences*, 15(4), 1291-1306.

490 Ma, Y., Wang, Y., Wu, R., Hu, Z., Yang, K., Li, M., . . . Chen, X. (2009). Recent advances on the study of
491 atmosphere-land interaction observations on the ~~tibetan~~[Tibetan](#) plateau. *Hydrology and Earth System Sciences*,
492 13(7), 1103-1111.

493 Mauder, M., Jegede, O., Okogbue, E., Wimmer, F., & Foken, T. (2007). Surface energy balance measurements at
494 a tropical site in [West africa](#)~~Africa~~ during the transition from dry to wet season. *Theoretical and Applied*
495 *Climatology*, 89(3-4), 171-183.

496 Sánchez, J., Caselles, V., & Rubio, E. (2010). Analysis of the energy balance closure over a FLUXNET boreal
497 forest in Finland. *Hydrology and Earth System Sciences*, 14(8), 1487-1497.

498 Scholes, R., Gureja, N., Giannecchini, M., Dovie, D., Wilson, B., Davidson, N., . . . Freeman, A. (2001). The
499 environment and vegetation of the flux measurement site near ~~skukuza~~[Skukuza](#), ~~kruger~~[Kruger](#) ~~n~~[National](#) ~~p~~[Park](#).
500 *Koedoe-African Protected Area Conservation and Science*, 44(1), 73-83.

501 Scholes, R. J., Bond, W. J., & Eckhardt, H. C. (2003). Vegetation dynamics in the [kruger](#)~~Kruger~~ ecosystem The
502 *Kruger Experience*. Island Press.

503 Shugart, H., Macko, S., Lesolle, P., Szuba, T., Mukelabai, M., Dowty, P., & Swap, R. (2004). The SAFARI 2000–
504 Kalahari transect wet season campaign of year 2000. *Global Change Biology*, 10(3), 273-280.

505 Stull, R. B. (2012). *An introduction to boundary layer meteorology* (Vol. 13): Springer Science & Business Media.

506 Su, H., Schmid, H. P., Grimmond, C., Vogel, C. S., & Oliphant, A. J. (2004). Spectral characteristics and
507 correction of long-term eddy-covariance measurements over two mixed hardwood forests in non-flat
508 terrain. *Boundary-Layer Meteorology*, 110(2), 213-253.

509 Twine, T. E., Kustas, W., Norman, J., Cook, D., Houser, P., Meyers, T., . . . Wesely, M. (2000). Correcting eddy-
510 covariance flux underestimates over a grassland. *Agricultural and Forest Meteorology*, 103(3), 279-300.

511 Von Randow, C., Manzi, A., Kruijt, B., De Oliveira, P., Zanchi, F., Silva, R., . . . Waterloo, M. (2004).
512 Comparative measurements and seasonal variations in energy and carbon exchange over forest and pasture in
513 south west ~~amazonia~~[Amazonia](#). *Theoretical and Applied Climatology*, 78(1-3), 5-26.

514 Wilczak, J. M., Oncley, S. P., & Stage, S. A. (2001). Sonic anemometer tilt correction algorithms. *Boundary-*
515 *Layer Meteorology*, 99(1), 127-150.

516 Williams, C. A., Hanan, N., Scholes, R. J., & Kutsch, W. (2009). Complexity in water and carbon dioxide fluxes
517 following rain pulses in an [African](#) savanna. *Oecologia*, 161(3), 469-480.

518 Wilson, K., Goldstein, A., Falge, E., Aubinet, M., Baldocchi, D., Berbigier, P., . . . Field, C. (2002). Energy
519 balance closure at FLUXNET sites. *Agricultural and Forest Meteorology*, 113(1), 223-243.

520 Xin, X., & Liu, Q. (2010). The two-layer surface energy balance parameterization scheme (TSEBPS) for
521 estimation of land surface heat fluxes. *Hydrology and Earth System Sciences*, 14(3), 491-504.

522 Yuling, F. (2005). Energy balance closure at ChinaFLUX sites.

523 [Zuo, J. Q., Wang, J. M., Huang, J. P., Li, W., Wang, G., & Ren, H. \(2011\). Estimation of ground heat flux and its](#)
524 [impact on the surface energy budget for a semi-arid grassland. *Sci Cold Arid Region*, 3, 41-50.](#)

525

526

527

Table 1: Measurements taken and instruments used at Skukuza flux tower

Instrument	Model/ brand	Measurement
Sonic anemometer	Gill Instruments Solent R3, Hampshire, England	3-dimensional, orthogonal components of velocity (u, v, w (ms^{-1})), sonic temperature
Closed path gas analyser	IRGA, LiCOR 6262, LiCOR, Lincoln	Water vapor, carbon dioxide concentrations
Radiometer	Kipp and Zonen CNR1, Delft, The Netherlands	Incoming and outgoing longwave and shortwave radiation
HFT3 plates	Campbell Scientific	Soil heat flux at 5 cm depth with 3 replicates, i.e. two under tree canopies and one on open space
Frequency domain reflectometry probes	Campbell Scientific CS615, Logan, Utah	Volumetric soil moisture content with two in the Acacia – dominated soils downhill of the tower at 3, 7, 16, 30, and 50 cm, and another two at 5, 13, 29, and 61 cm in the Combretum – dominated soils uphill

528

529

530

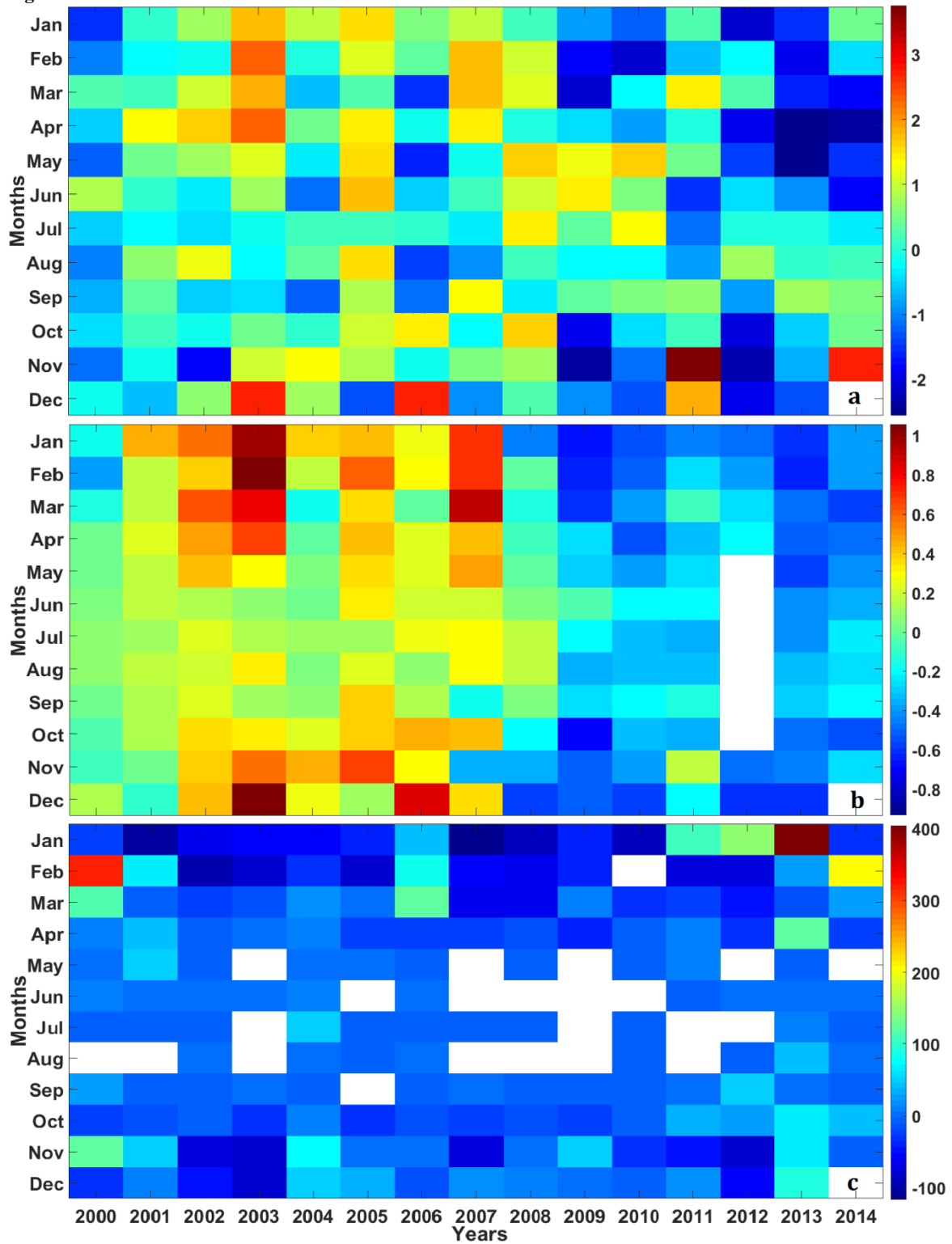
Table 2: Statistical summary of annual values of the energy balance components

Year	% data completion		H	LE	G	Rn
2000	14.16	Max	470.31	422.89	191.53	817.60
		Min	-139.77	-72.43	-61.60	-95.93
		Mean	45.82	36.11	5.32	91.46
2001	12.78	Max	790.82	513.09	292.87	899.90
		Min	-159.87	-85.95	-90.27	-116.58
		Mean	58.56	43.68	9.27	128.27
2002	17.77	Max	415.93	174.07	171.93	583.30
		Min	-117.66	-89.16	-86.00	-122.21
		Mean	61.35	10.29	4.10	90.72
2003	41.50	Max	556.21	308.71	217.60	879.30
		Min	-92.99	-97.81	-106.23	-116.04
		Mean	58.15	21.68	6.17	94.53
2004	28.21	Max	505.36	498.10	129.96	925.30
		Min	-150.08	-89.07	-69.76	-5.88
		Mean	56.46	17.99	7.97	156.10
2005	35.37	Max	606.28	737.43	288.20	933.20
		Min	-130.40	-97.00	-107.37	-4.92
		Mean	51.43	17.82	0.99	159.09
2006	7.59	Max	583.66	331.25	335.30	1003.30
		Min	-72.45	-119.09	-72.80	-6.56
		Mean	84.67	35.94	19.69	247.70
2007	48.77	Max	552.93	426.34	340.67	1011.30
		Min	-131.40	-130.79	-129.70	-6.71
		Mean	59.04	14.32	4.14	169.84
2008	54.30	Max	616.43	439.76	238.57	1038.50
		Min	-140.13	-144.97	-104.60	-5.91
		Mean	63.06	26.30	6.22	191.26
2009	42.69	Max	551.34	776.62	328.93	1060.50
		Min	-96.68	-135.43	-94.20	-155.90
		Mean	55.42	96.54	6.87	207.77
2010	57.65	Max	626.68	624.38	199.33	888.00
		Min	-173.11	-135.62	-66.35	-180.70
		Mean	57.23	52.54	3.74	105.10
2011	41.34	Max	591.16	688.46	171.27	832.00
		Min	-135.77	-127.02	-58.59	-96.50
		Mean	63.88	73.11	1.75	127.94
2012	27.62	Max	572.11	566.88	185.80	899.00
		Min	-171.83	-148.49	-50.92	-99.69
		Mean	59.25	52.49	2.16	111.31
2013	67.97	Max	570.79	665.48	146.03	845.58
		Min	-197.40	-149.10	-55.36	-107.70
		Mean	50.25	38.63	-1.22	92.80
2014	28.66	Max	533.46	726.31	89.50	893.00
		Min	-238.65	-134.39	-33.36	-89.70
		Mean	59.37	69.55	1.18	147.30

534 Figures

535

536 Figures



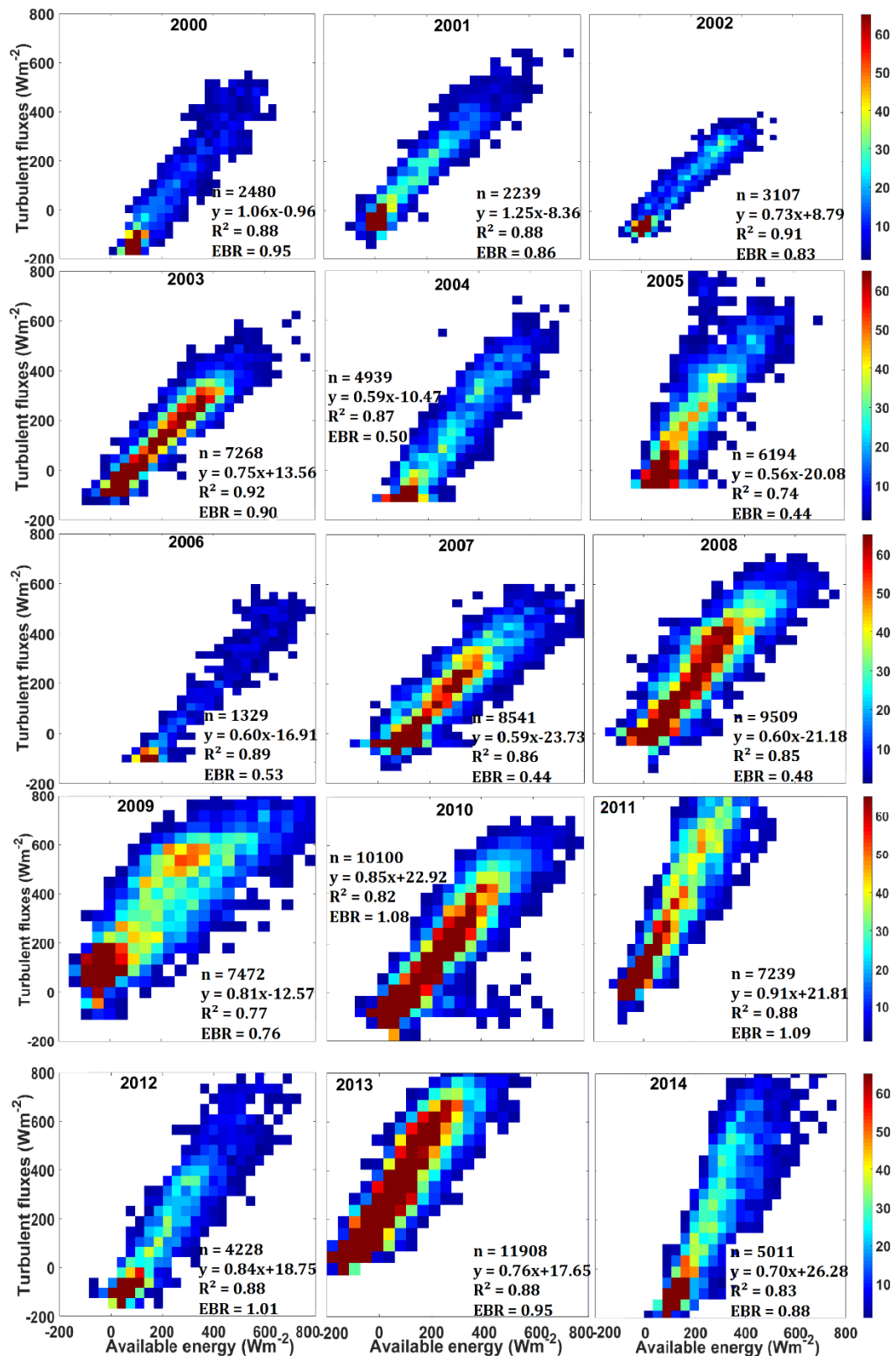
537

538

539

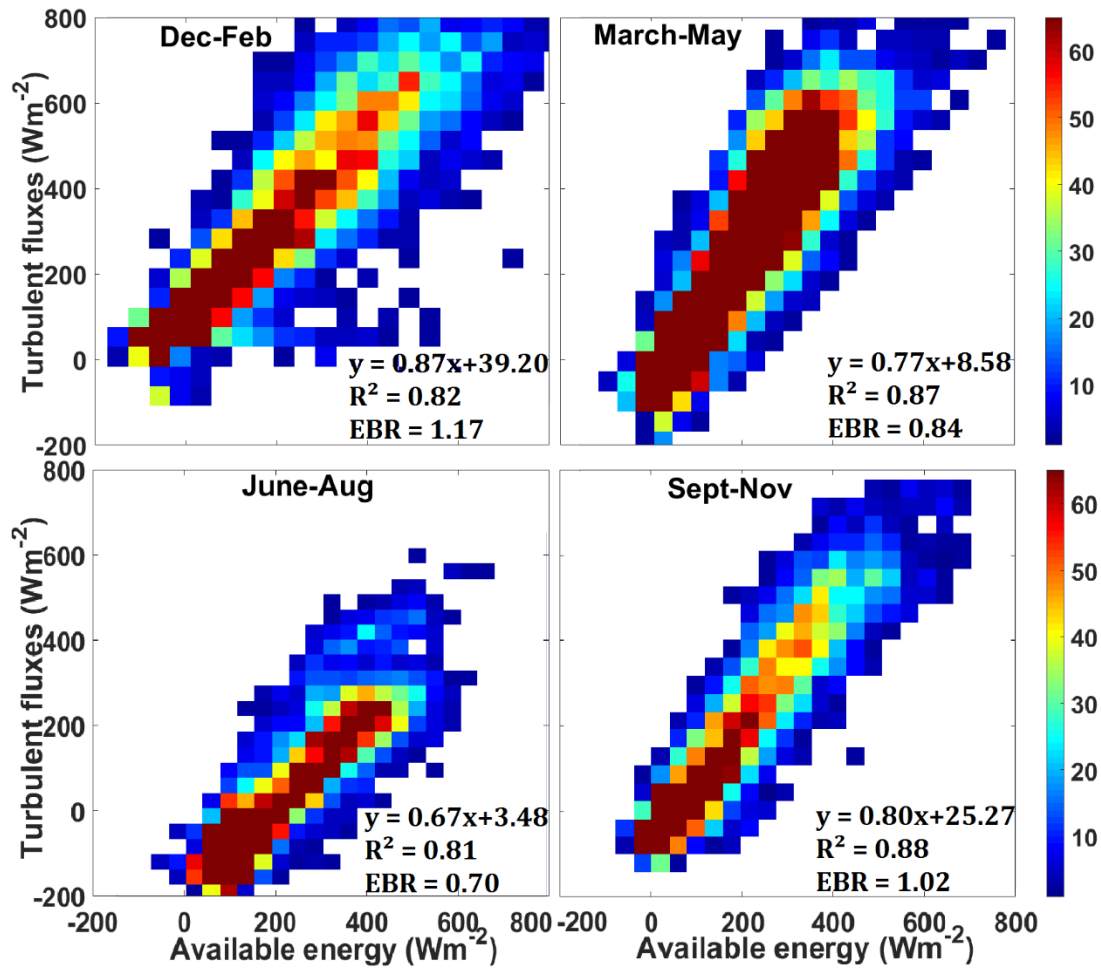
Figure 1: summaries of daily-mean monthly anomalies (a) average-air temperature, (b) average-VPD, and (c) total rainfall from 2000 to 2014

540



541
542
543
544

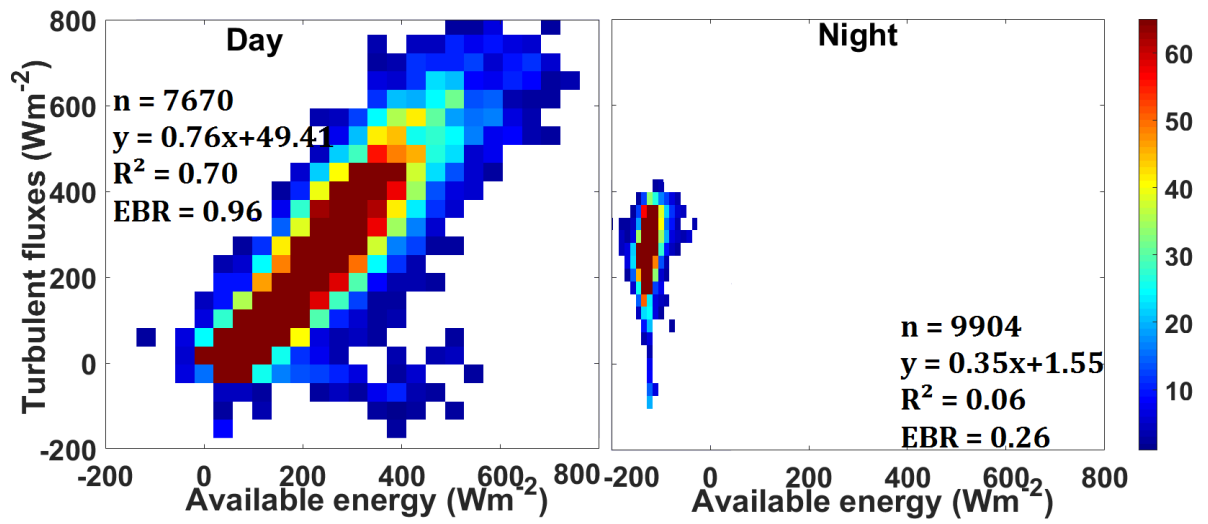
Figure 2: 15-year series of annual regression analysis of turbulent (sensible and latent) heat fluxes against available energy (net radiation minus ground-conduction heat flux) from 2000 to 2014 at Skukuza, (SA). The colour bars represent the count of EBR values.



545

546 Figure 3: Seasonal turbulent fluxes (H+LE) correlation to available energy (Rn-G) for Skukuza flux tower from
 547 summer(Dec-Feb), autumn (March-May), winter (June-Aug), spring (Sept-Nov). The colour bars represent the count
 548 of EBR values

549

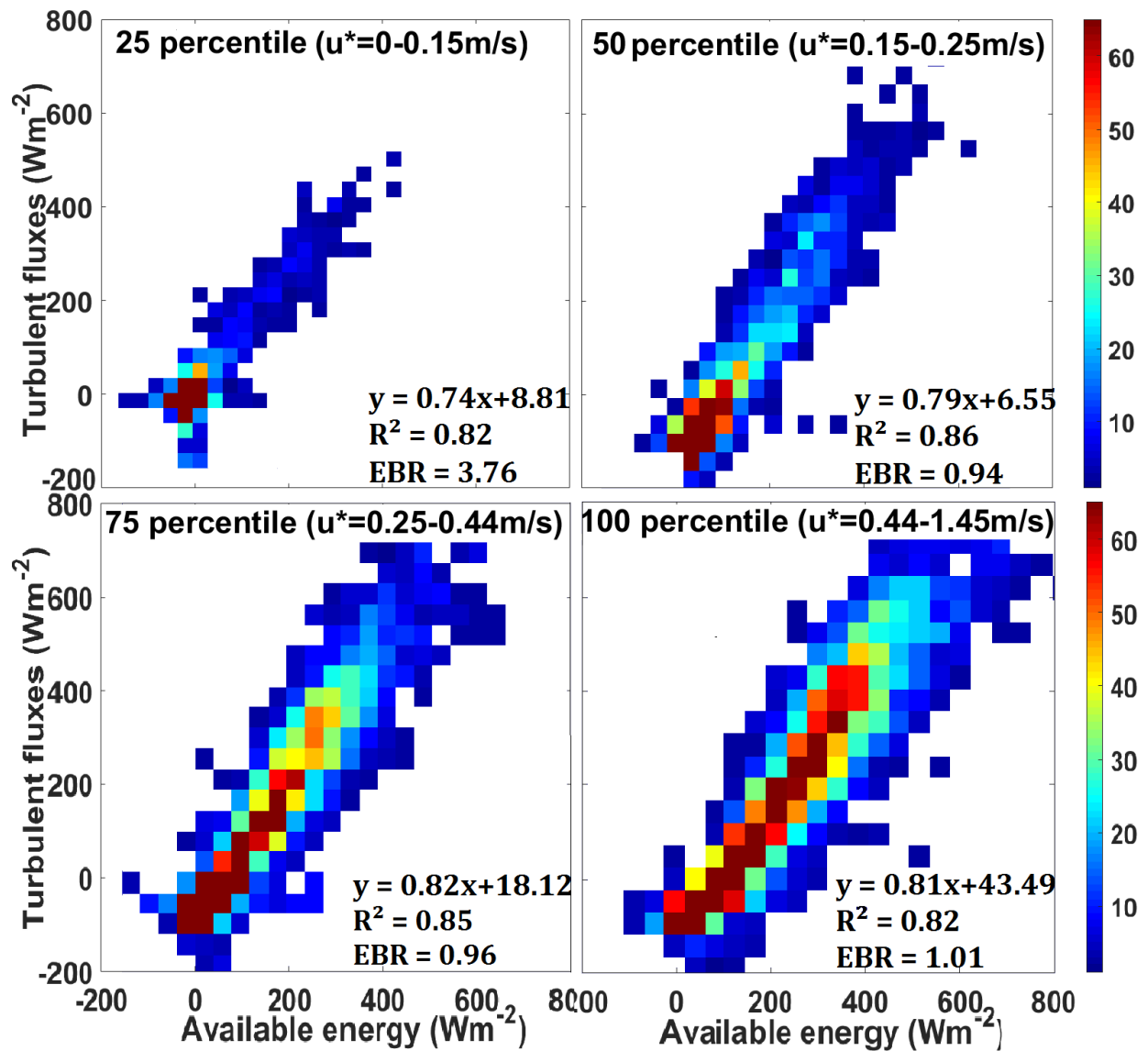


550
551
552

Figure 4: Turbulent fluxes correlation to available energy for daytime (a) and night-time (b), using the full (2000-2014) 15-year available data series. The colour bars represent the count of EBR values

553

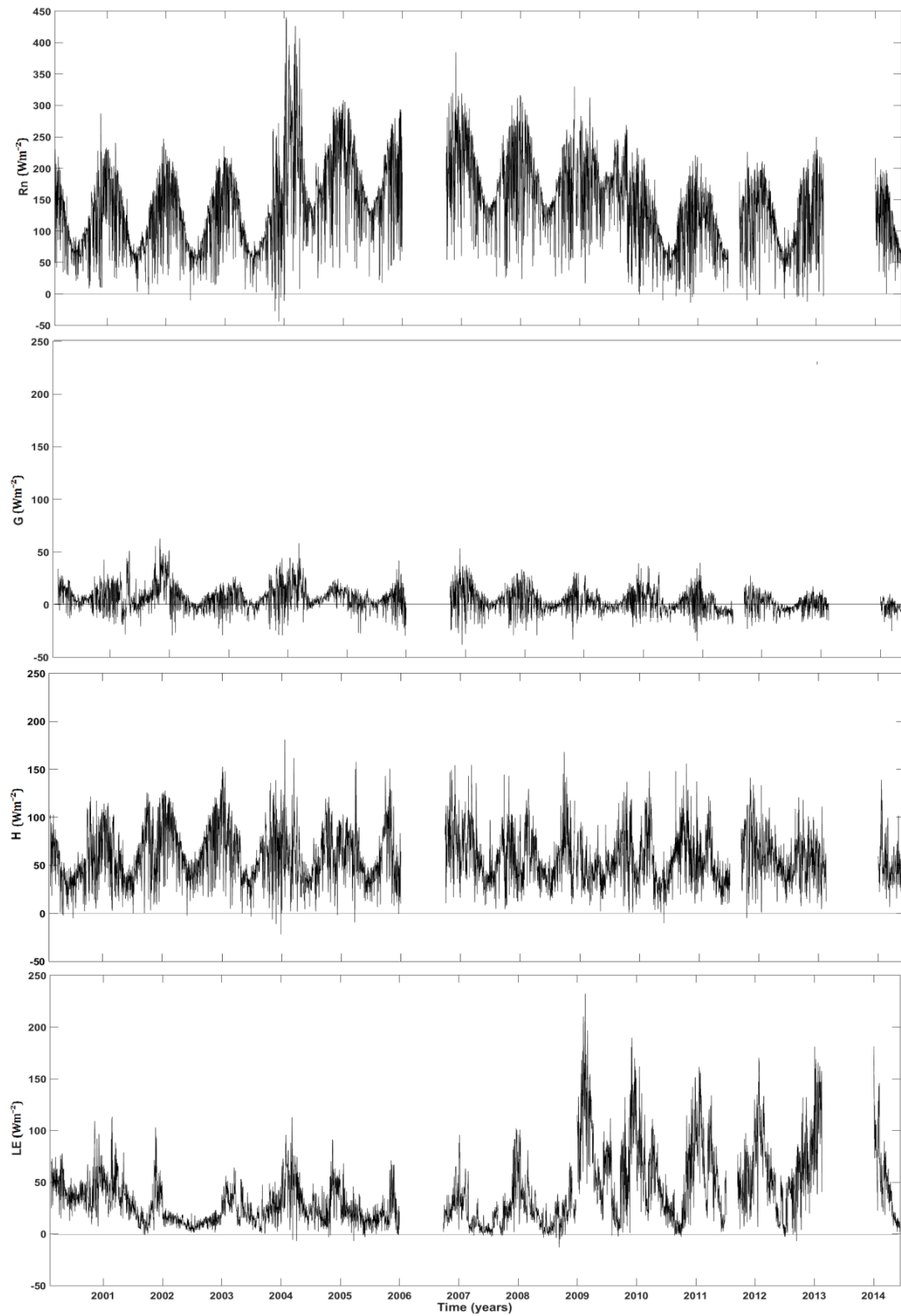
554



555
556
557

Figure 5: OLS and EBR evaluations at different friction velocity sorted at 4 quartiles. The colour bar represents the count of EBR values. The colour bars represent the count of EBR values.

558
559
560

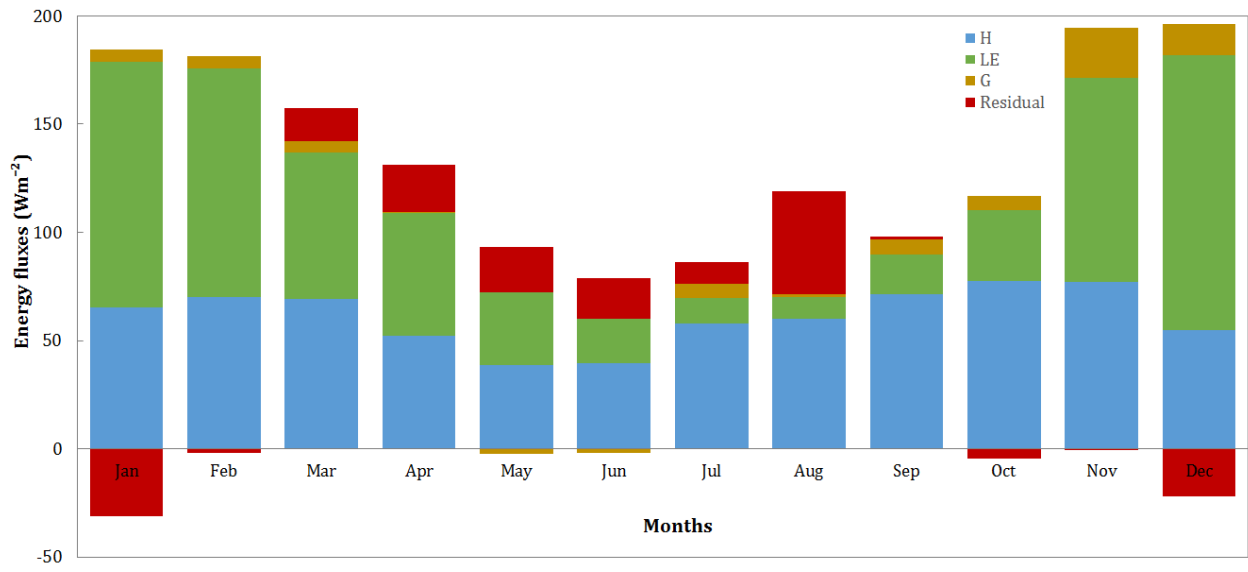


561
562
563

Figure 6: Time series of daily mean surface energy balance component fluxes from 2000 to 2014 at Skukuza flux tower site (SA)

564

565



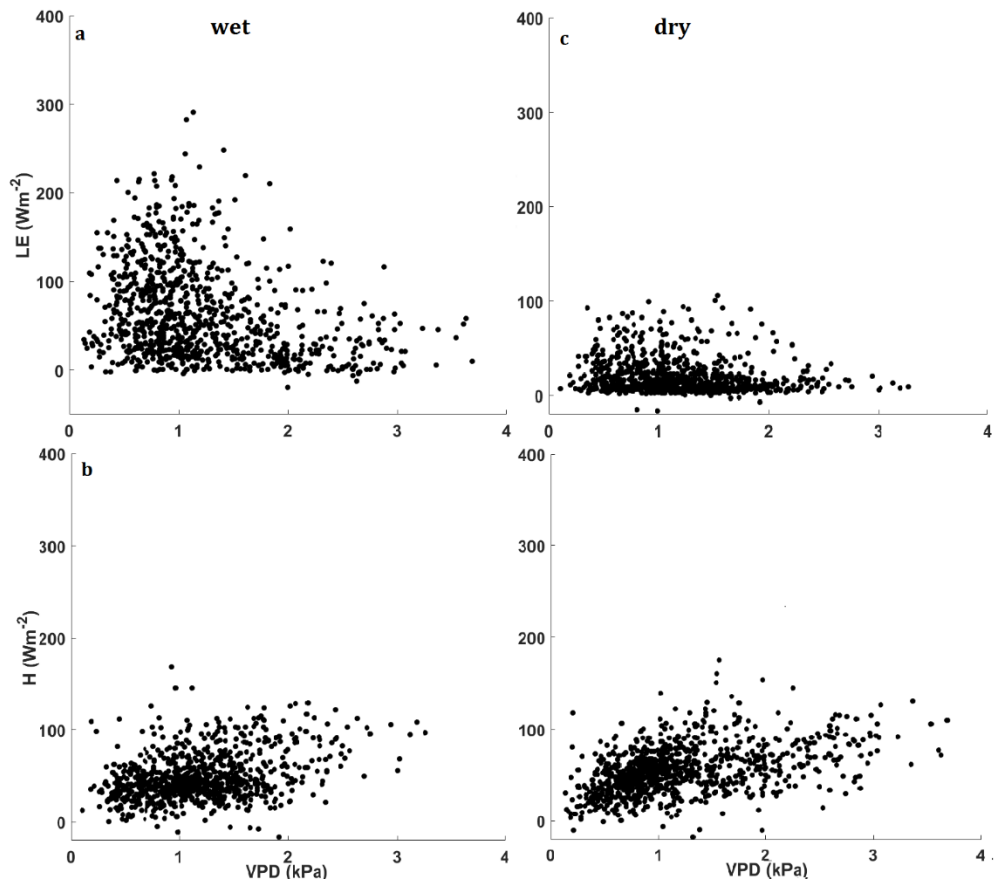
566

567

568

Figure 7: 15-year (2000-2014) monthly means of surface energy balance fluxes of Skukuza flux tower site (SA), highlighting the partitioning of R_n

569

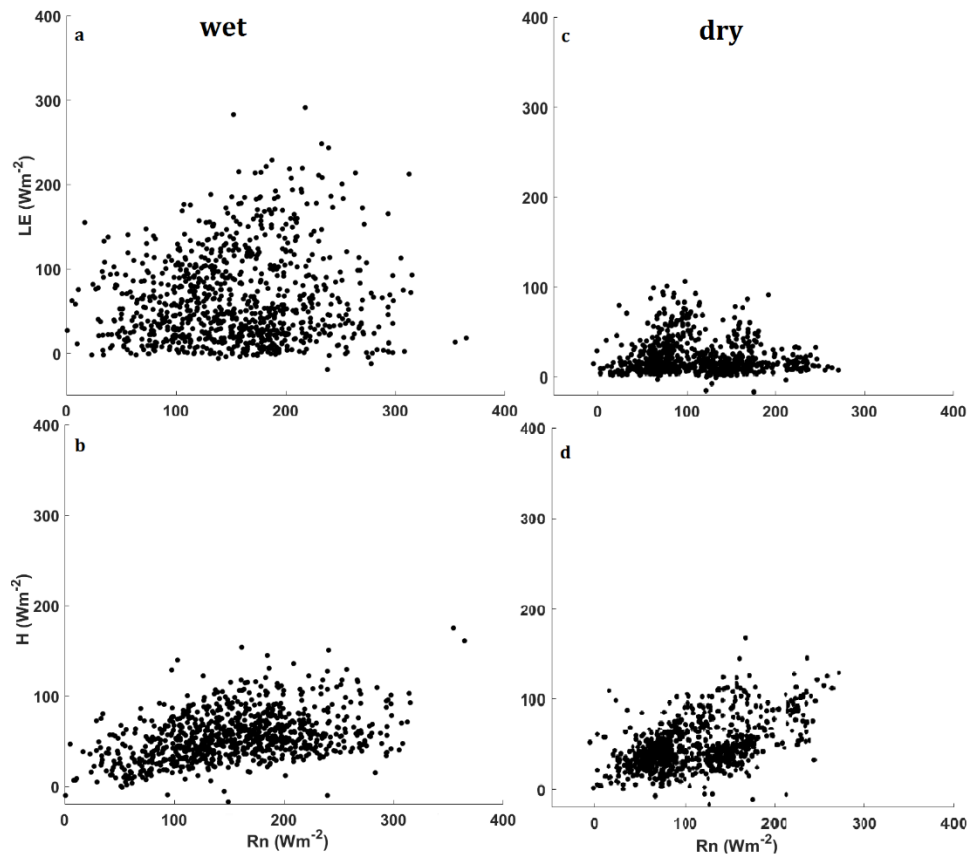


570

571

Figure 8: Relationship between the fluxes and VPD under wet and dry conditions

572



573
574

Figure 9: Effects of net radiation on LE and H under wet and dry conditions

575